Diffraction Tomography

Malcolm Slaney and A.C.Kak

School of Electrical Engineering
Purdue University
West Lafayette, IN 47907

Abstract

This paper reviews diffraction tomography as it applies to electromagnetic and acoustical imaging. We have discussed the various approximations that are used and shown their effects by computer simulation. In addition results are shown for three reconstruction algorithms and their computational requirements are explored.*

1. Introduction

During the past ten years the medical community has increasingly called on X-Ray computerized tomography (CT) to help make its diagnostic images. With this increased interest has also come an awareness of the dangers of using ionizing radiation and this has made X-Ray CT unsuitable for use in mass screening of the female breast, for example.

For this reason researchers have turned to microwaves and acoustics as possible imaging modalities. While at low levels microwaves and ultrasound are considered safe, they both suffer from diffraction effects in biological tissue. In the past these problems have been ignored [Cra82] or approximated using digital ray tracing [And82]. A complete solution requires the theory of inverse scattering and has been labelled "Diffraction Tomography."

This paper will discuss several of the problems that must be solved for diffraction tomography to produce acceptable images. We will first discuss a scattering model and two of the approximations that must be made will then be presented. In the third section we will formulate the forward process which will be inverted in section 4 to give us an estimate of the imaging parameter of the object. We will also present computer simulation results to illustrate the effects of the approximations made.

In section 5 we will discuss several of the algorithms used for diffraction tomography and compare the resulting reconstructions both from the standpoint of accuracy and the computing effort required. This will be followed in sections 6 by a discussion of several of the experimental limitations and a derivation of the optimum sampling interval.

2. The Wave Equation

We will discuss the inverse scattering problem in terms of the scalar Helmholtz equation. Diffraction tomography algorithms are derived from the following general equation for wave propagation in an inhomogeneous medium

$$(\nabla^2 + k^2)\psi(\vec{r}) = -O(\vec{r})\psi(\vec{r}) \tag{2.1}$$

where $\psi(\vec{r})$ represents the scalar field. The wavenumber, k, is calculated from the average properties of the medium and thus $O(\vec{r})$ is a function of the deviations of the medium from the average.

For the acoustic case, first order approximations give the following expression for $O(\vec{r})$ [Kak83],

$$O(\vec{r}) = k^2[n^2(\vec{r})-1] \tag{2.2}$$

where $n(\vec{r})$ is the refractive index of each point in the object. On the other hand, if we ignore the effect of polarization, the function $O(\vec{r})$ for the electromagnetic case is given by

*This work was supported by the Walter Reed Army Institute of Research.

$$O(\vec{r}) = 2k^2[n(\vec{r})-1] \tag{2.3}$$

where $n(\vec{r})$ is

$$n(\vec{r}) = \sqrt{\frac{\mu(\vec{r})\epsilon(\vec{r})}{\mu_0\epsilon_0}}. \tag{2.4}$$

Here we have used μ and ϵ to represent the magnetic permeability and dielectric constant and the subscript zero to indicate their average values.

The incident field, ψ_0, is a solution to the homogeneous Helmholtz equation

$$(\nabla^2+k^2)\psi_0(\vec{r}) = 0. \tag{2.5}$$

The total field may be represented as a sum of the incident field, $\psi_0(\vec{r})$, and the scattered field, $\psi_s(\vec{r})$,

$$\psi(\vec{r}) = \psi_0(\vec{r})+\psi_s(\vec{r}). \tag{2.6}$$

From (2.1) and (2.6) we see that $\psi_s(\vec{r})$ satisfies the following wave equation

$$(\nabla^2+k^2)\psi_s(\vec{r})=-O(\vec{r})\psi(\vec{r}). \tag{2.7}$$

The scalar Helmholtz equation (2.1) cannot be solved for $\psi_s(\vec{r})$ directly but a solution can be written in terms of a Green's function [Mor53]. The Green's function, which is a solution of the differential equation

$$(\nabla^2+k_0^2)G(\vec{r}|\vec{r}\,') = -\delta(\vec{r}-\vec{r}\,'), \tag{2.8}$$

is written as

$$G(\vec{r}|\vec{r}\,') = \frac{e^{jkR}}{4\pi R} \tag{2.9}$$

with

$$R = |\vec{r}-\vec{r}\,'|. \tag{2.10}$$

In two dimensions the solution of (2.8) is written in terms of a zero-order Hankel function of the first kind, and can be expressed as

$$G(\vec{r}|\vec{r}\,') = \frac{i}{4}H_0^{(1)}(kR). \tag{2.11}$$

Since equation (2.8) represents the radiation from a two-dimensional impulse source, the total radiation from all sources on the right hand side of (2.7) must be given by the following superposition:

$$\psi_s(\vec{r}) = \int G(\vec{r}|\vec{r}\,')O(\vec{r}\,')\psi(\vec{r}\,')d\vec{r}\,'. \tag{2.12}$$

Since in general, it is impossible to solve equation (2.12) for the scattered field, approximations must be made. Two types of appoximations are available: the Born and the Rytov. For the first order Born approximation the integral equation of (2.12) is solved by assuming that the total field, $\psi(\vec{r})$, differs only slightly from the incident field and therefore the total field can be approximated by the incident field, $\psi_0(\vec{r})$,

$$\psi_s(\vec{r}) \simeq \int G(\vec{r}|\vec{r}\,')O(\vec{r}\,')\psi_0(\vec{r}\,')d\vec{r}\,'. \tag{2.13}$$

Due to R in equation (2.10) being a function of the difference $\vec{r}-\vec{r}\,'$, this may be expressed as the following two-dimensional convolution

$$\psi_s(\vec{r}) \simeq \int G(\vec{r}-\vec{r}\,')O(\vec{r}\,')\psi_0(\vec{r}\,')d\vec{r}\,'. \tag{2.14}$$

The first order Born approximation is valid only when the magnitude of the scattering is small compared to the incident field. When this is true the incident field is a close approximation to the total field in the integral of equation (2.12). It can be shown [Sla82] that one condition for this to be true is that the total phase shift in the incident field as it passes through object must be less than π.

Higher order approximations for the total field ψ are possible with the Born approach. The total field is now represented as

$$\psi(\vec{r}) = \psi_0(\vec{r}) + \psi_1(\vec{r}) + \psi_2(\vec{r}) + \cdots \tag{2.15}$$

We have already presented an equation for the first order scattering term ($\psi_1=\psi_s$) in equation (2.14). Higher order terms are given by

$$\psi_{i+1}(\vec{r}) \simeq \int G(\vec{r}-\vec{r}\,')O(\vec{r}\,')\psi_i(\vec{r}\,')d\vec{r}\,'. \tag{2.16}$$

More work is needed to determine the region of convergence for this series.

The Rytov approximation is derived by assuming that the total field can be expressed as a complex phase or

$$\psi(\vec{r}) = e^{jk\phi(\vec{r})}. \tag{2.17}$$

The total phase is then expressed as

$$\phi(\vec{r}) = \phi_0(\vec{r}) + \phi_s(\vec{r}). \tag{2.18}$$

Substituting this new expression for the total field into the inhomogeneous Helmholtz equation (2.1) and simplifying by subtracting out the effect of the homogeneous solution we find that [Ish78, Che60]

$$\psi_0(\vec{r})\phi_s(\vec{r}) = \int G(\vec{r}-\vec{r}\,')\psi_0(\vec{r}\,')\left[\nabla\phi_s\cdot\nabla\phi_s + O(\vec{r}\,')\right]d\vec{r}\,'. \tag{2.19}$$

Under the Rytov solution we assume that the term in brackets can be approximated by only the object term or

$$\nabla\phi_s\cdot\nabla\phi_s + O(\vec{r}\,') \simeq O(\vec{r}\,') \tag{2.20}$$

The Rytov solution to the scattered field then becomes

$$\phi_s(\vec{r}) = \frac{1}{\psi_0(\vec{r})}\int G(\vec{r}-\vec{r}\,')\psi_0(\vec{r}\,')O(\vec{r}\,')d\vec{r}\,' \tag{2.21}$$

or comparing to equation (2.14)

$$\phi_s(\vec{r}) = \frac{\psi_s(\vec{r})}{\psi_0(\vec{r})} \tag{2.22}$$

Contrary to the Born approximation the Rytov approximation assumes that the term $\nabla\phi_s\cdot\nabla\phi_s$ is small compared to the object function, $O(\vec{r}\,')$. This condition is equivalent to saying that the change in the scattered field per unit length must be small. Since no assumptions were made about the size of the object the Rytov approximation is considered to be a better approximation to the true fields [Kel69].

The similarity between the expressions for the first order Born and Rytov solutions will form the basis of our reconstructions. In the Born approximation we measure the complex amplitude of the scattered field and use this as an estimate of the function ψ_s while in the Rytov case we estimate ψ_s from the phase of the scattered field. Since the Rytov approximation is considered more accurate than the Born approximation it should provide a better estimate of ψ_s.

3. The Forward Process

Let us consider the effect of a single plane wave incident on the object. The forward scattered field will be measured at the receiver line as is shown in figure 1.

A single plane wave in two dimensions can be represented as

$$\psi_0(\vec{r}) = e^{j\vec{k}\vec{r}} \tag{3.1}$$

where $\vec{k} = (k_x, k_y)$ satisfies the following relationship

$$k^2 = k_x^2 + k_y^2. \tag{3.2}$$

Let us now consider the scattered field from an object, $O(\vec{r})$, by analyzing equation (2.13) in the Fourier domain. We will use the plots of figure 2 to illustrate the various transformations that take place.

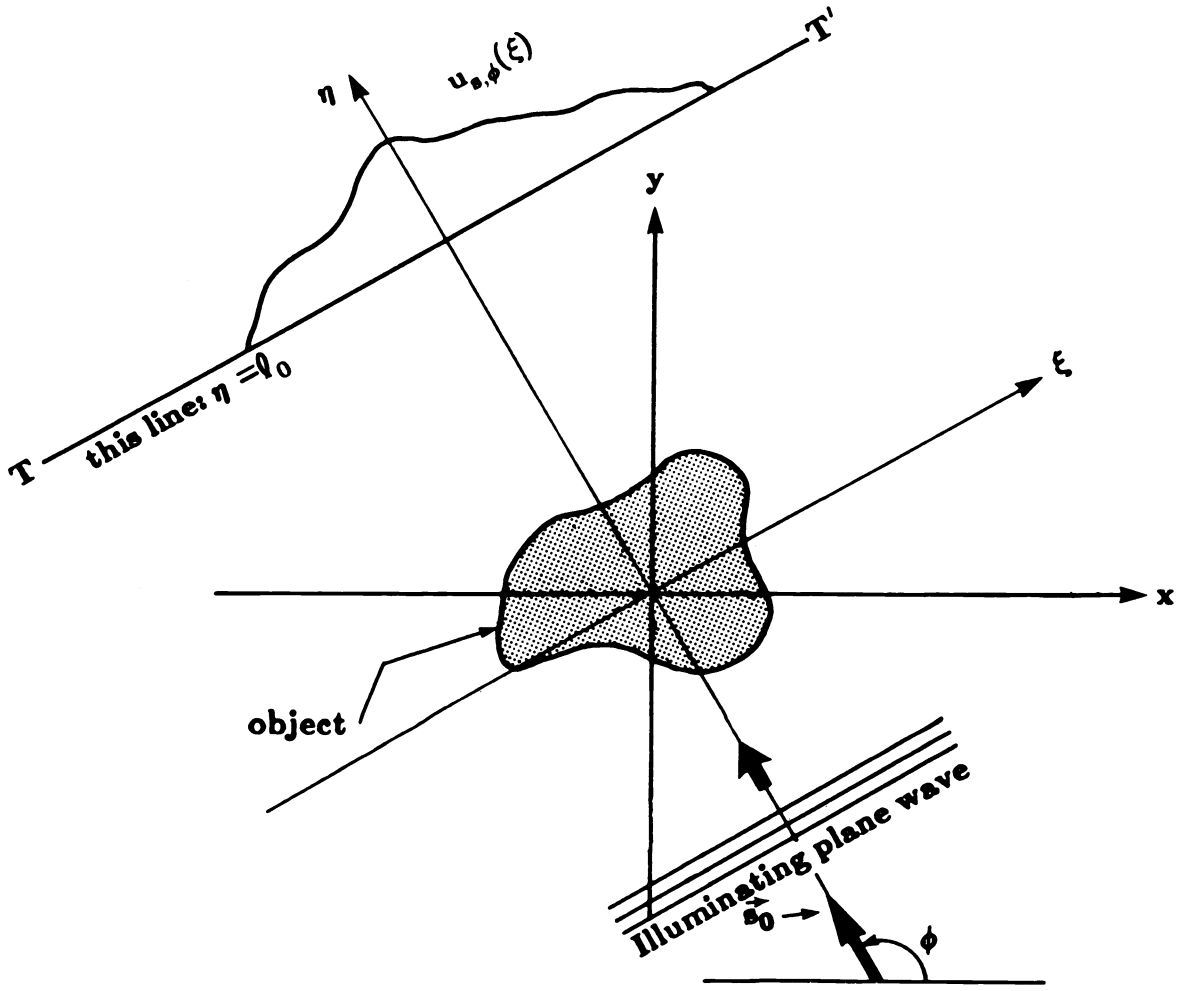

Figure 1. A simple diffraction tomography experiment

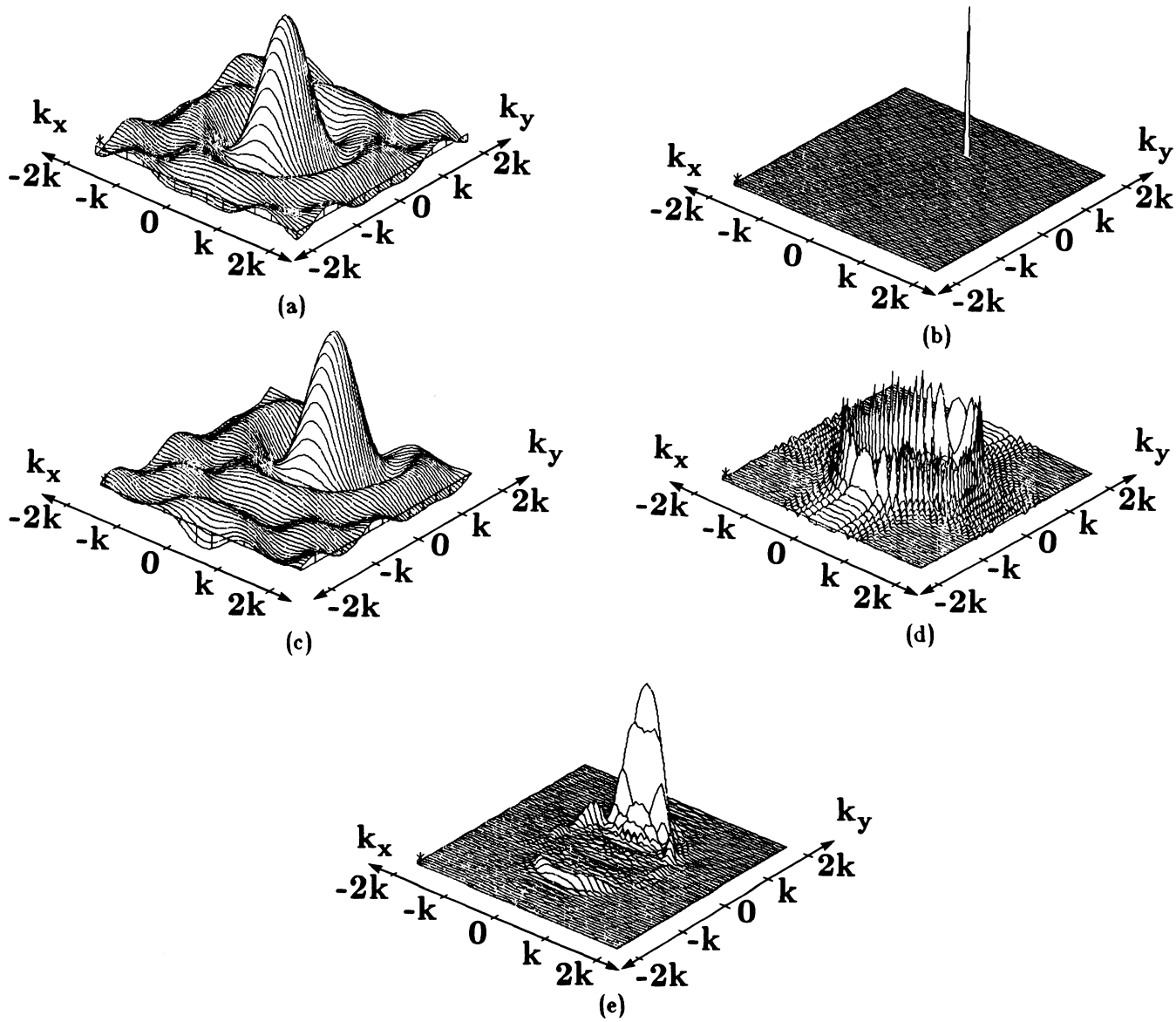

Figure 2. Several of the Fourier tranforms involved in the calculation of the scattered field. a) The Fourier transform of the object, b) the Fourier transform of the incident field, c) the convolution (in the frequency domain) of (a) and (b), d) the Fourier Transform of the 2D Green's function and (e) the Fourier transform of the first order Born scattered field.

The integral equation for the scattered field (2.13) can be considered as a convolution of the Green's Function, $G(\vec{r}|\vec{r}\,')$, and the product of the object function $O(\vec{r})$, and the incident field, $\psi_0(\vec{r})$. First we will define the following Fourier transform pairs.

$$O(\vec{r}) \leftrightarrow \tilde{O}(\vec{k}) \tag{3.3}$$

$$G(\vec{r}-\vec{r}\,') \leftrightarrow \tilde{G}(\vec{k}) \tag{3.4}$$

$$\psi(\vec{r}) \leftrightarrow \tilde{\psi}(\vec{k}) \tag{3.5}$$

Equation (2.14) can now be written in terms of these Fourier transforms or

$$\tilde{\psi}_s(\vec{\Lambda}) = \tilde{G}(\vec{\Lambda})\left\{\tilde{O}(\vec{\Lambda}) * \tilde{\psi}_0(\vec{\Gamma})\right\} \tag{3.6}$$

where we have used '*' to represent convolution and $\vec{\Lambda} = (\alpha,\gamma)$. In equation (3.1) we presented an expression for ψ_0. It's Fourier transform is given by

$$\tilde{\psi}_0(\vec{\Lambda}) = 2\pi\delta(\vec{\Lambda}-\vec{k}) \tag{3.7}$$

and thus the convolution of equation (3.6) becomes a shift in the frequency domain or

$$\tilde{O}(\vec{\Lambda}) * \tilde{\psi}_0(\vec{\Gamma}) = 2\pi\tilde{O}(\vec{\Lambda}-\vec{k}). \tag{3.8}$$

This convolution is illustrated in figures 2a-c for a plane wave propogating with direction vector, $\vec{k}=(0,k)$. Figure 2a shows the Fourier transform of a single cylinder of radius 1λ and figure 2b is the Fourier Transform of the incident field. The resulting multiplication in the space domain or convolution in the frequency domain is shown in figure 2c.

Taking the Fourier transform of equation (2.8) it follows that the Fourier transform of the Green's function is [Mor53]

$$G(\vec{\Lambda}|\vec{r}\,') = \frac{e^{-j\vec{k}\vec{r}\,'}}{\Lambda^2-k^2}. \tag{3.9}$$

This function has a singularity for all $\vec{k}$ such that

$$\Lambda^2 = \alpha^2+\gamma^2 = k^2. \tag{3.10}$$

An approximation to $G(\vec{k})$ is shown in figure 2d.

The effect of the convolution shown in equation 2.14 is a multiplication in the frequency domain of the shifted object function, (3.8), and the Green's function, (3.9), evaluated at $\vec{r}\,' = 0$. The scattered field is written as

$$\tilde{\psi}(\vec{\Lambda}) = 2\pi\frac{\tilde{O}(\vec{\Lambda}-\vec{k})}{\Lambda^2-k^2}. \tag{3.11}$$

This result is shown in figure 2e for a plane wave propogating along the y-axis. Since the largest frequency domain components of the Green's function satisfy equation (3.10) the Fourier transform of the scattered field is dominated by a shifted and sampled version of the object's Fourier transform.

We will now derive an expression for the field at the receiver line. For simplicity we will assume that the incident field is propagating along the positive y axis or $\vec{k} = (0,k)$. The scattered field along the receiver line $(x, y = l_0)$ is simply the inverse Fourier transform of the field in equation (3.11). This is written as

$$\psi(x, y=l_0) = \frac{1}{4\pi^2}\int\int \tilde{\psi}_s(\vec{\Lambda}) e^{j\vec{\Lambda}\cdot\vec{r}}\, d\alpha\, d\gamma \tag{3.12}$$

which, using (3.11), can be expressed as

$$\psi_s(x, y=l_0) = \frac{1}{4\pi^2}\int\int \frac{\tilde{O}(\alpha,\gamma-k)}{\alpha^2+\gamma^2-k^2} e^{j(\alpha x+\gamma l_0)}\, d\alpha\, d\gamma. \tag{3.13}$$

In order to evaluate this inversion it is necessary to perform contour integration, choosing the path of integration to lead to outgoing waves [Mor53]. Performing the contour integration with respect to γ we find

$$\psi(x,y=l_0) = \int\left\{\frac{\tilde{O}(\alpha,\gamma-k)e^{j\gamma l_0}}{j2\gamma}\right\}e^{j\alpha x}\,d\alpha. \tag{3.14}$$

Defining

$$\tilde{U}(\alpha) = \frac{\tilde{O}(\alpha,\gamma-k)}{j2\gamma}e^{j\gamma l_0} \tag{3.15}$$

we can write equation (3.14) as

$$\psi(x,y=l_0) = \int \tilde{U}(\alpha)e^{j\alpha x}\,d\alpha \tag{3.16}$$

or

$$\int \psi(x,y=l_0)e^{-j\alpha x}\,dx = 2\pi\tilde{U}(\alpha). \tag{3.17}$$

Thus the Fourier transform of the received field is a simple function of the Fourier transform of the object along a circular arc. This is diagramed in figure 3. This can be further justified by noting that in figure 2e, only those frequencies that satisfy equation (3.10) will be propogated to the receiver line [Goo68].

This result was first presented by Wolf [Wol69]. Devaney [Dev82] later extended this result to show that in the limit of very small wavelengths that this result approaches the formulas used in X-ray CT imaging [Ros82].

We have derived an expression (3.17) that relates the scattering by an object to the field received at a line. Within the diffraction limit it is possible to invert this relation to estimate the object scattering distribution based on the received field. Because of diffraction effects it is only possible to receive waves with a wavenumber such

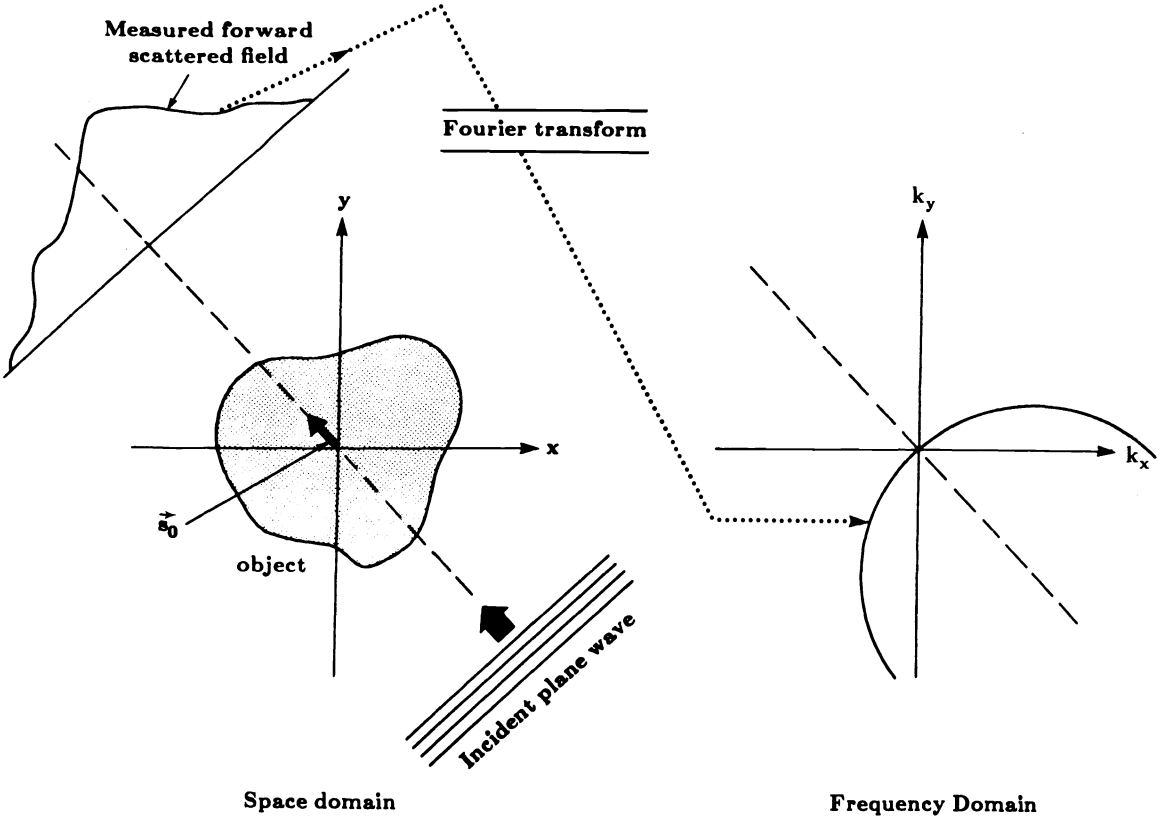

Figure 3. The measured scattered field is an estimate of the Fourier transform of the object along a circular arc.

that both α and γ are real. If either part of the wavenumber is complex then this component of the field will be exponentially attenuated and will be negligible at distances greater than 10λ. This limits the wavenumbers of the received field to those such that

$$\alpha \leq k \tag{3.18}$$

and thus

$$\gamma = \sqrt{k^2-\alpha^2} \leq k. \tag{3.19}$$

Within this limitation, the relationship between the object function and the received field is exact.

4. Inversion

In order to estimate an object, its Fourier transform must be known for all frequencies in a neighborhood of the origin. We have shown how the scattered field from an object provides an estimate of the Fourier transform of the object along a circular arc. In order to obtain an estimate of the object for all frequencies within a disk it is necessary to change the incident field and the object's orientation.

There are two different approaches that are currently being investigated. The most straightforward was discussed by Mueller [Mue79] and consists of rotating the object and measuring the scattered field for different orientations. Each orientation will produce an estimate of the object's Fourier transform along a circular arc and these arcs will rotate as the object is rotated. When the object has rotated through a full 360 degrees an estimate of the object will be available for the entire Fourier disk.

The coverage for this method is shown in figure 4. Notice that there are two arcs that pass through each point of Fourier space. Generally it will be necessary to choose one estimate as better.

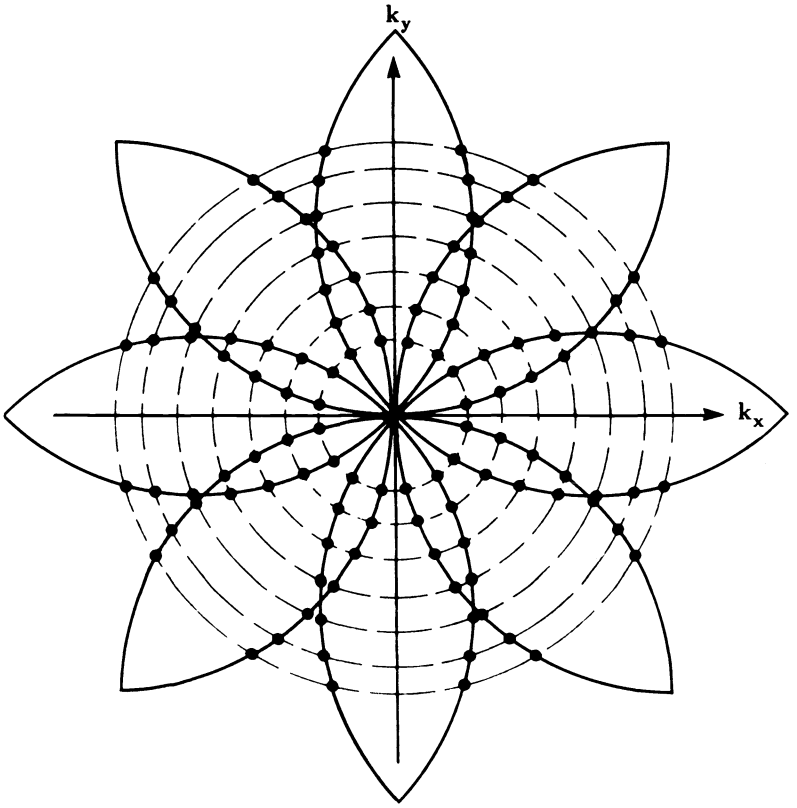

Figure 4. Frequency domain coverage. Each arc represents a single diffracted projection.

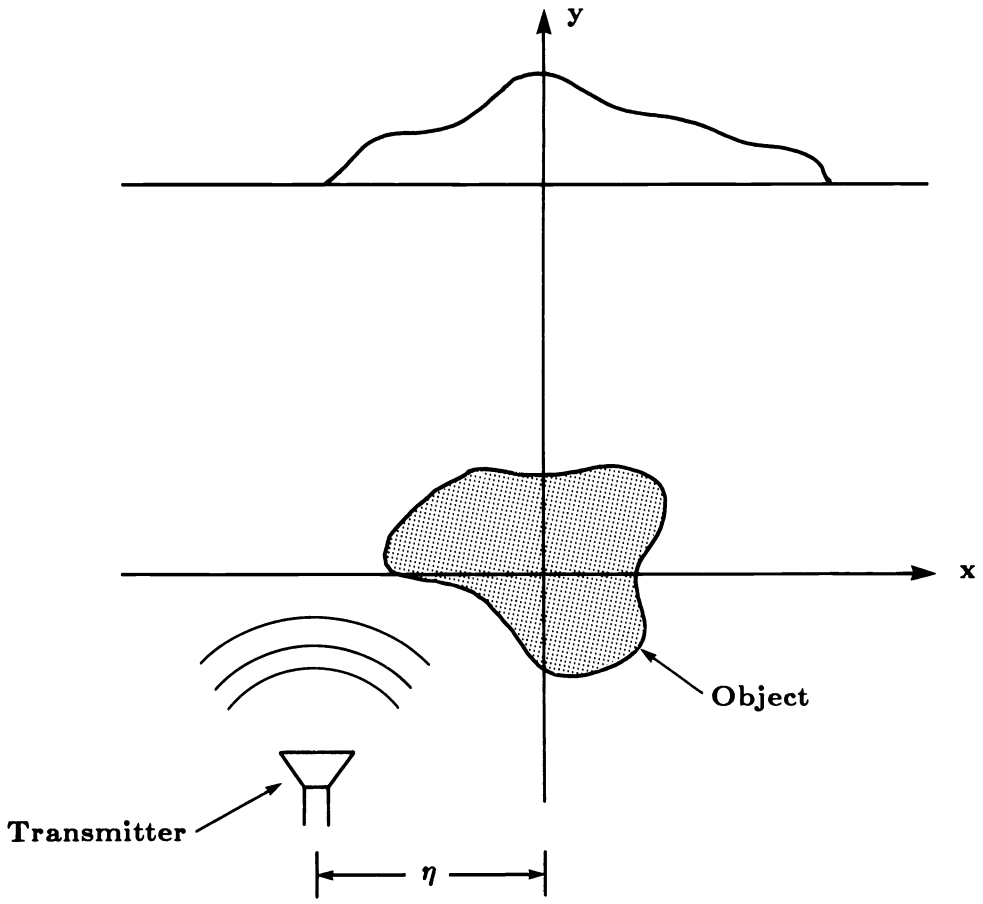

Figure 5. An experiment using the approach of [Nah82] is shown here. A single view consists of measuring the diffracted projections for every possible position, η, of the transmitter.

Nahamoo and Kak [Nah82] have proposed a method that requires only two rotational views of an object. Consider an arbitrary source of waves in the transmitter plane as is shown in figure 5. The field produced can be represented as a set of plane waves by taking the Fourier transform of the transmitter aperture function [Goo68]. Doing this we find

$$\psi_t(x) = \frac{1}{4\pi^2}\int_{-\infty}^{\infty} A_t(k_x)e^{jk_x x}\,dk_x. \tag{4.1}$$

Moving the source to a new position, η, we find that the plane wave decomposition becomes

$$\psi_t(x+\eta) = \frac{1}{4\pi^2}\int_{-\infty}^{\infty}\left(A_t(k_x)e^{jk_x\eta}\right)e^{jk_x x}\,dk_x. \tag{4.2}$$

Given the plane wave decomposition the incident field in the plane follows simply as

$$\psi_i(\eta;x,y) = \int_{-\infty}^{\infty}\left(\frac{1}{4\pi^2}A_t(k_x)e^{jk_x\eta}\right)e^{j(k_x x+k_y y)}\,dk_x. \tag{4.3}$$

In equation (3.11) we presented an equation for the scattered field from a single plane wave. Because of the

linearity of the Fourier transform we can write the Fourier transform of the total scattered field due to the incident field $\psi_i(x+\eta)$ as [Nah82]

$$\tilde{\psi}_s(\eta;\alpha) = \int_{-\infty}^{\infty} A_i(k_x) e^{jk_x\eta} \frac{\tilde{O}(\alpha-k_x,\gamma-k_y)}{j2\gamma} dk_x. \tag{4.4}$$

Taking the Fourier transform of both sides with respect to the transmitter position, η, we find that

$$\tilde{\psi}_s(k_x;\alpha) = A_i(k_x) \frac{\tilde{O}(\alpha-k_x,\gamma-k_y)}{j2\gamma} k_x. \tag{4.5}$$

By collecting the scattered field along the receiver line as a function of transmitter position, η, we have an expression for the scattered field. Like the simpler case with plane wave incidence, the scattered field is related to the Fourier transform of the object along an arc. Unlike the previous case, though, the coverage due to a single view of the object is a pair of circular disks as shown in figure 6. Here a single view is defined as consisting of transmitting from all positions in a line and measuring the scattered field at all positions along the receiver line. By rotating the object by 90 degrees it is possible to generate the complimentary disk and to fill the Fourier domain.

Several simulations were done comparing and contrasting the Born and Rytov approximations. The resulting reconstructions are shown in figures 7-9. Both the Born and Rytov solutions produced excellent results for the

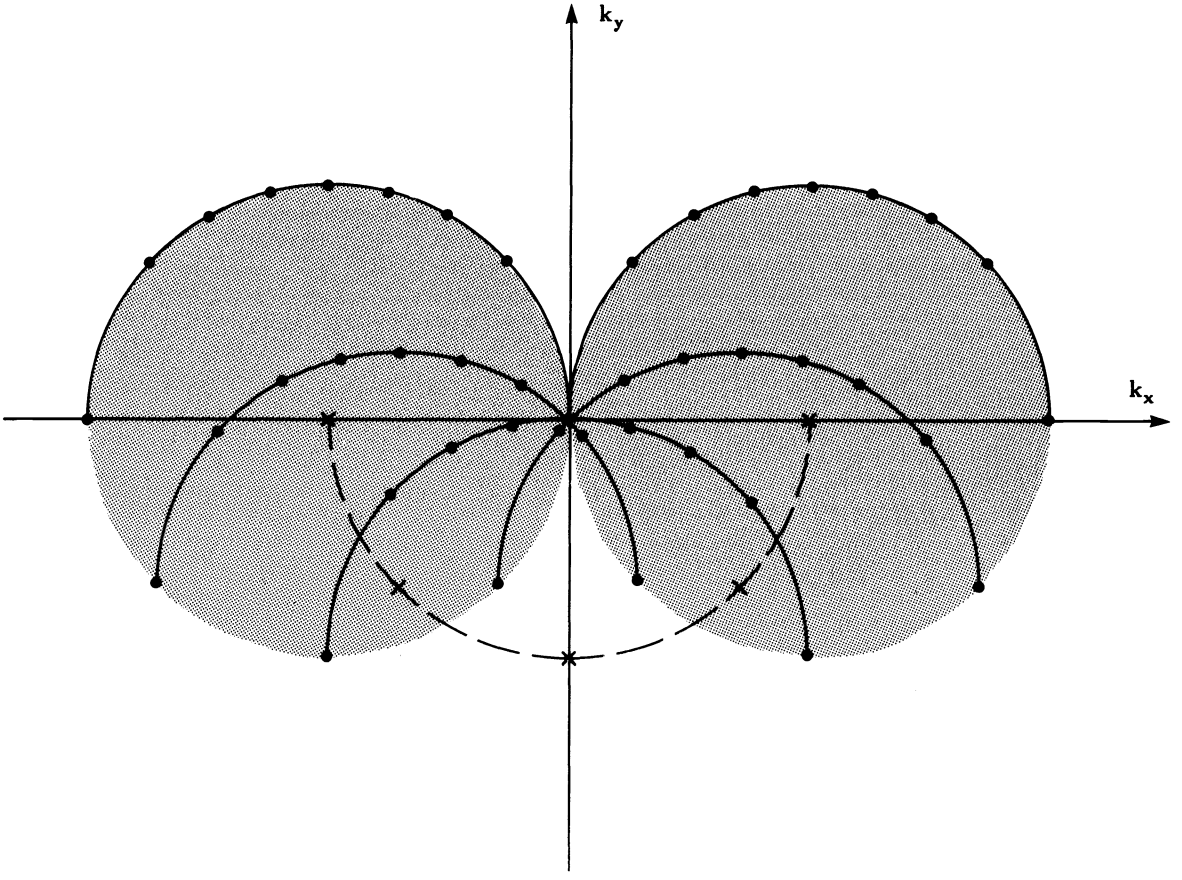

Figure 6. The object coverage in the Fourier domain for synthetic aperature tomography. The dotted semicircle represents the possible incident waves while the othersemicircles are the possible received waves.

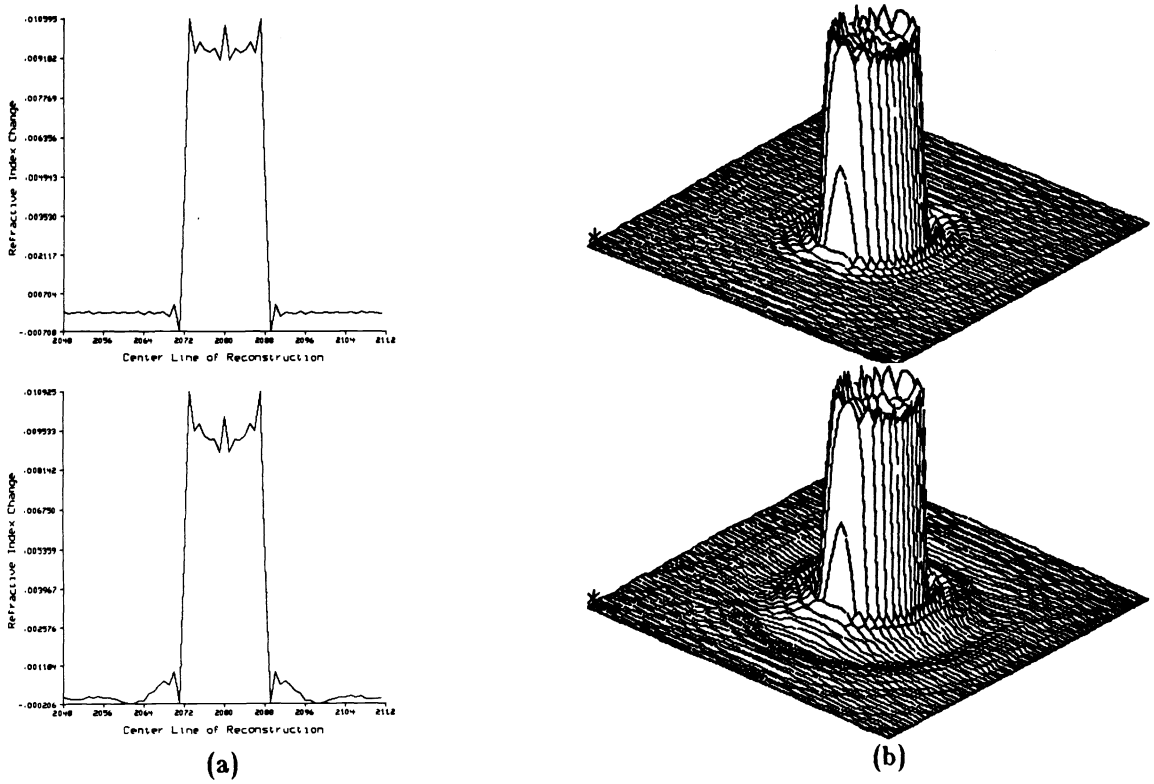

(a) (b)

Figure 7. Reconstructions of a 4λ cylinder with a refractive index of 1.01. Maximum phase shift across the object is 1.6π. (a) Born approximation, and (b) Rytov approximation.

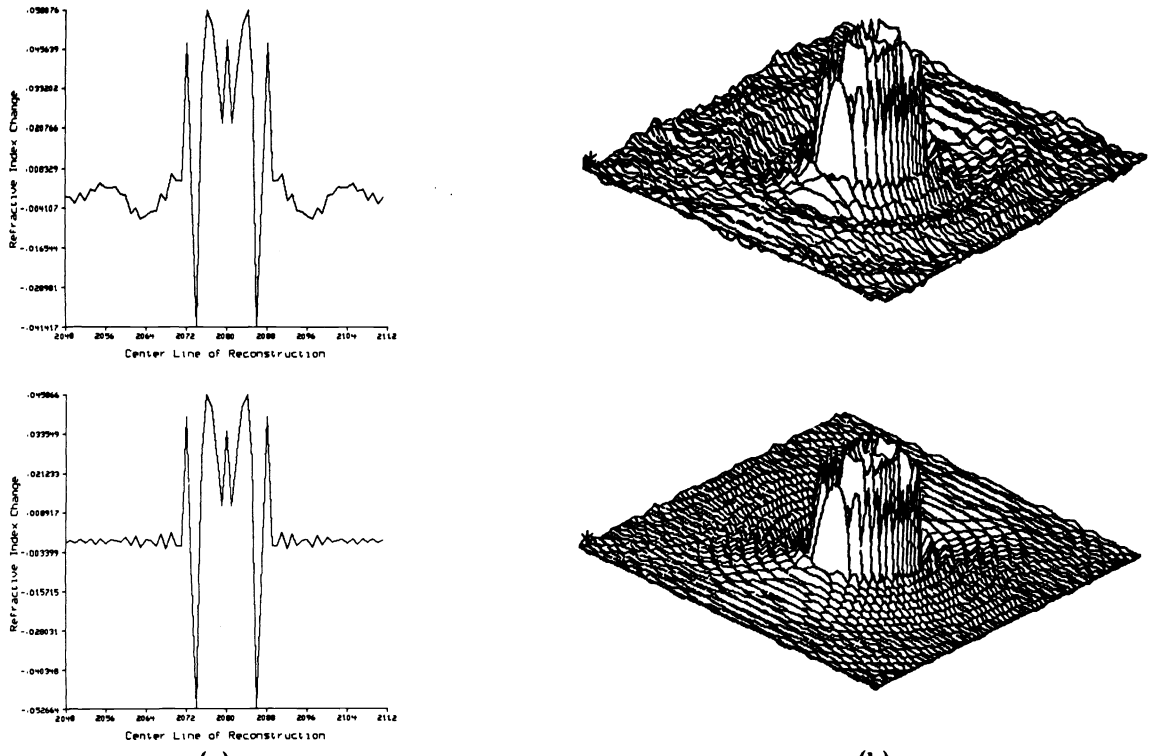

(a) (b)

Figure 8. Reconstructions of a 4λ cylinder with a refractive index of 1.20. Maximum phase shift across the object is 3.2π. (a) Born approximation, and (b) Rytov approximation.

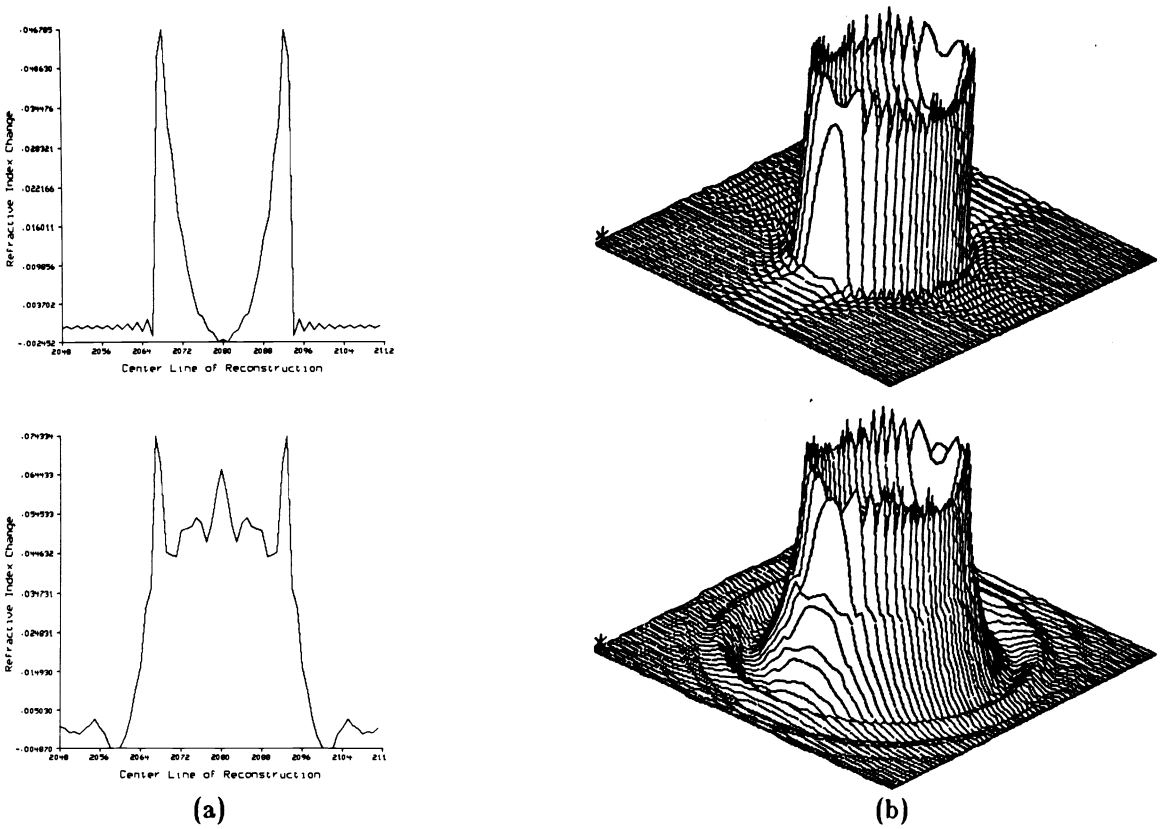

Figure 9. Reconstructions of a 40λ cylinder with a refractive index of 1.005. Maximum phase shift across the object is .8π. (a) Born approximation, and (b) Rytov approximation.

relatively uninteresting case of a .1% change in refractive index. On the other hand neither approximation produced a good reconstruction for a 20% change. Figure 9 highlights the difference between the Born and Rytov approximations for a .5% change. Notice that while the Born approximation produced a better estimate of the step refractive index the overall reconstruction is not as good as the Born approximation. This is consistent with the limitations of each approximation as presented above.

5. Reconstruction Algorithms

Exactly estimating the scattered field for every point within the Fourier disk would require an infinite amount of data so generally the scattered field is measured only for a finite number of views and receiver positions. In addition the object is usually sampled using a rectangular grid so that an FFT based algorithm can be used to find its inverse. It it then necessary to estimate the Fourier transform at discrete points in the frequency domain given an estimate of the Fourier transform along circular arcs.

We will discuss several reconstruction algorithms as they apply to the simple plane wave incidence. Similar reconstructions can also be derived for the approach presented in [Nah82] but the math is not nearly as straightforward.

In order to estimate the Fourier transform of the object for points on a rectangular grid it would be simplest to choose enough views so that every point in the grid is on one of the scattered arcs. This is generally not reasonable because of the large number of views this implies.

A much more reasonable approach is to use two dimensional interpolation to estimate the Fourier transform of the object function from the data collected along circular arcs in the frequency domain. Several techniques can be used for interpolation. These include nearest neighbor (the simplest and least accurate), bilinear interpolation, and zero padding the signal to increase the resolution of the Fourier transform. The application of these ideas is discussed in [Pan83].

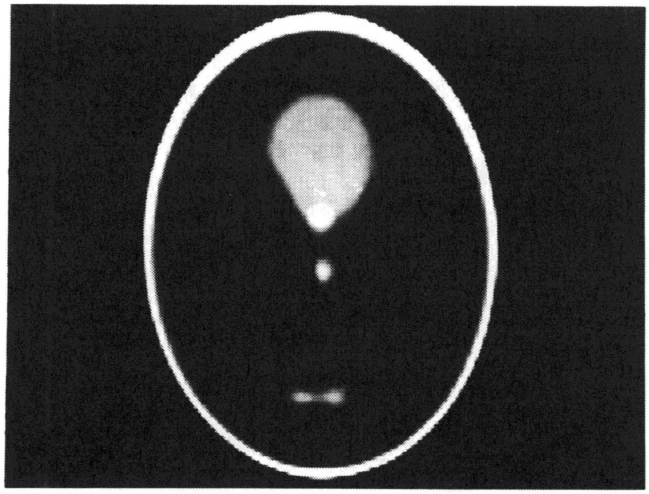

(a)

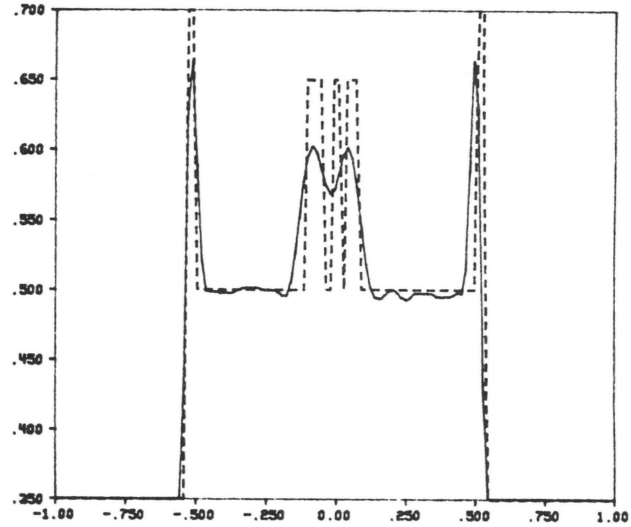

(b)

Figure 10. A 128 by 128 reconstruction obtatined with bilinear interpolation from 64 projects and 128 samples per projection. Prior to applying bilinear interpolation, the frequency domain sampling density was increased eightfold by the zero padding technique. (a) is the full reconstruction and (b) is a numerical comparison of the true and reconstructed values on the line y=-.605 through the phantom

Figure 10 shows simulations for a phantom similar to the Shepp and Logan X-ray CT skull phantom. Using a combination of increasing the sampling density by zero padding the signal and bilinear interpolation, results were obtained in 2 minutes of CPU time on a VAX 11/780 minicomputer with a floating point accelerator (FPA). The reconstructions were done over a 128 by 128 grid using 64 views and 128 receiver positions. The number of operations required to carry out the interpolation and invert the object function is on the order of $N^2 \log N$.

Devaney [Dev82] has derived a filter-backpropagation algorithm that directly calculates the object function without the need for interpolation and a two dimensional inverse FFT. The filtered-backpropagation algorithm differs from the filtered-backprojection algorithm in conventional tomography because the projection filter is different for each depth. This is diagrammed in figure 11. For the most accurate reconstruction it is necessary to backpropagate the field to every depth represented by the object array.

In Devaney's algorithm, the object function is reconstructed by

$$O(x,y) = \frac{k_0}{8\pi^2} \int_0^{2\pi} d\phi \int_{-k}^{k} d\alpha \, |\alpha| \, \Gamma_\phi(\alpha) e^{j(\gamma-k)(\eta-l_0)} e^{j\alpha\xi} \tag{5.1}$$

where ξ and η represent the rotated versions of the x and y coordinate system as shown in figure 5. The function, $\vec{\Gamma}_\phi$, is a function of the scattered field and the projection angle and is given by

$$\Gamma_\phi(\alpha) = \frac{j}{k_2} e^{-jkl_0} \tilde{U}_{s,\phi}(\alpha) \tag{5.2}$$

This calculation requires on the order of $N_\phi N_d N \log N$ operations where N_ϕ is the number of projections, N_d is the number of depths the backpropagation is performed and each projection consists of N values.

If only a small portion of the entire object is of interest, then it is possible to reduce the computational requirements by only backpropagating to a single depth. This method has been called the Modified Back Propagation Algorithm.

Pan and Kak [Pan83] presented the reconstructions shown in figures 12 and 13. Figure 12 represents the result of back propagating the data to 128 depths for each view while figure 13 is the result of back propagation to only a single depth centered near the three small ellipses at the bottom of the picture. The results were simulated on a

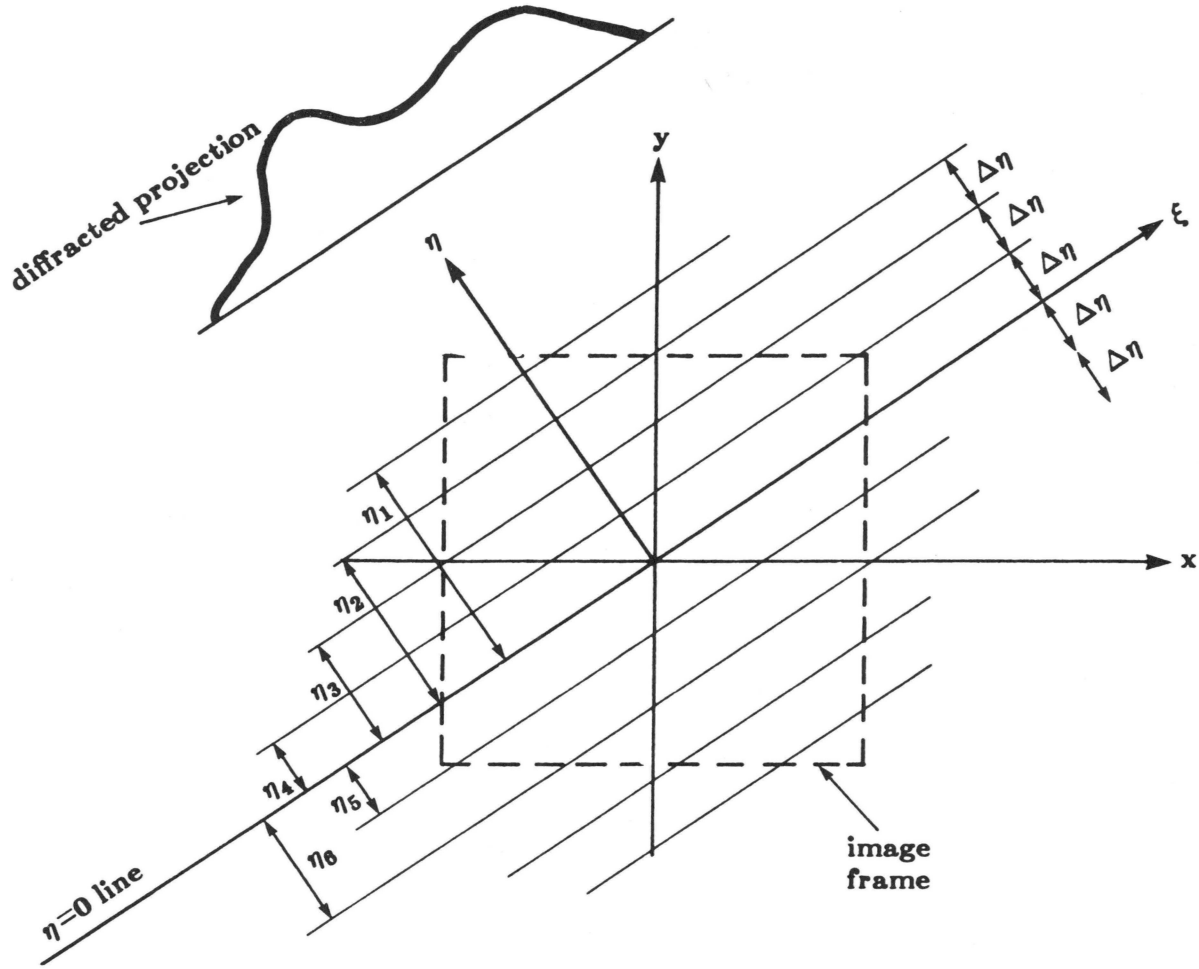

Figure 11. For each η-constant line shown in this figure, the diffracted projection must be filtered with a different transfer function.

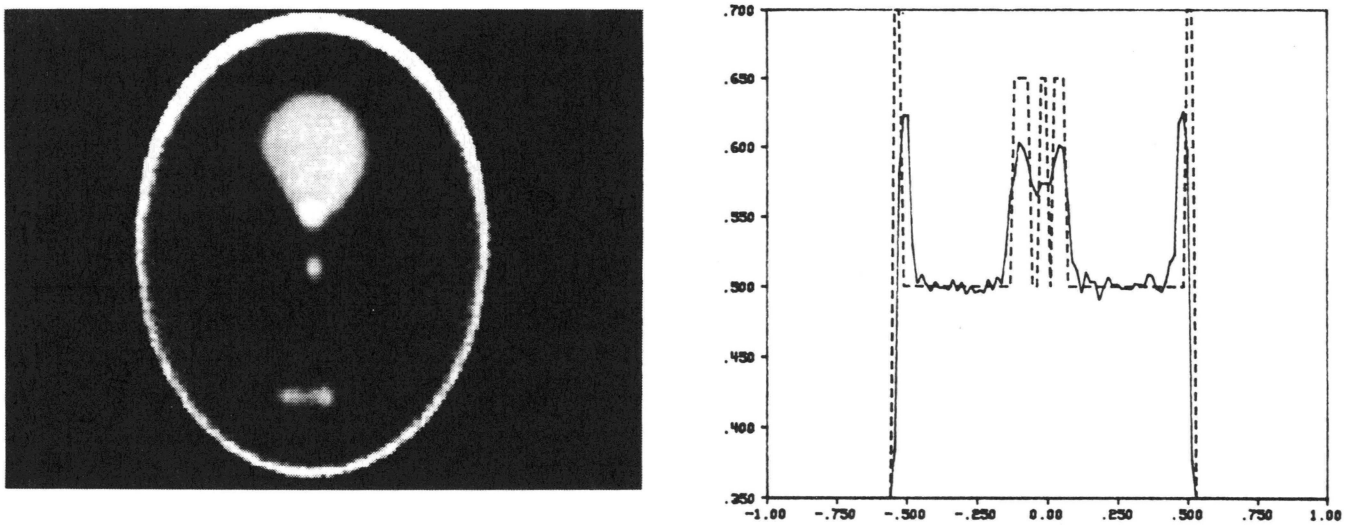

(a) (b)

Figure 12. Reconstructions obtained by using the filter-backpropagation algorithm on 64 projections and 128 samples in each projection. N_d=128.. (a) is the full reconstruction and (b) is a numerical comparison of the true and reconstructed values on the line y=-.605 through the phantom

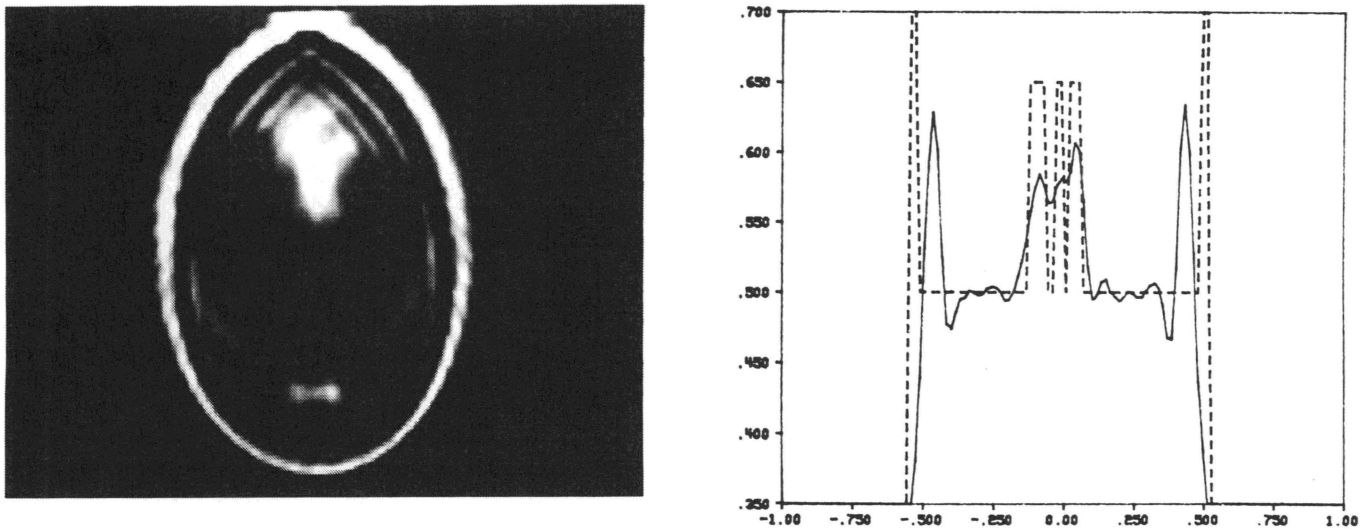

(a) (b)

Figure 13. Reconstructions obtained by using the modified filter-backpropagation algorithm on 64 projections and 128 samples in each projection. The filter function corresponds to what would yield local accuracy at the site of the three small ellipses. (a) is the full reconstruction and (b) is a numerical comparison of the true and reconstructed values on the line y=-.605 through the phantom

VAX 11/780 minicomputer and the resulting reconstructions were done over a 128 by 128 grid. Like the previous image the input data consisted of 64 projections of 128 points each.

There was a significant difference in not only the reconstruction time but also the resulting quality. While the modified back propagation only took 1.25 minutes the resulting reconstruction is much poorer than the full back propagation which took 50 minutes of CPU time.

6. Limitations

There are a number of limitations in diffraction tomography. We have already considered the limits of the Born and Rytov approximations. These serve to limit the maximum change in refractive index that can be imaged.

There are several other factors that limit the quality of reconstructions possible [Sla82]. The most fundamental limitations is due to the propagation of evanescent waves. Since these waves have a complex wavenumber [Goo68] they are severely attenuated as they propagate. Thus at a distance of more than 10 wavelengths their contribution to the total field is almost negligible.

The severe attenuation of the evanescent waves limits the highest frequency that can be measured at the receiver line. Since the field at the receiver line corresponds directly to the Fourier transform of the object this limits the highest frequency in the reconstruction.

In addition to the limitation on reconstruction bandwidth due to the propagation of evanescent waves the sampling interval and the number of data points collected along the receiver line effect the reconstruction. A simple Nyquist rate analysis shows that the reconstruction is limited to frequencies less than one half the sampling rate. Spatial frequencies higher than this will be aliased into the lower frequencies.

Measuring the scattered field in the near field also introduces a low pass filtering of the reconstruction. Consider the effect of the point scatter shown in figure 14. The scattered field that is measured at the receiver line is a function of the scatterer's distance from the receiver line and the angle of incidence. At a point, $(x,y=l_0)$ the scattered field is given by

$$U(x=l_0,y) = \frac{e^{jk\sqrt{x^2+y^2}}}{\sqrt{x^2+y^2}}. \qquad (6.1)$$

The instantaneous spatial frequency is found by taking the partial derivative of the phase with respect to y

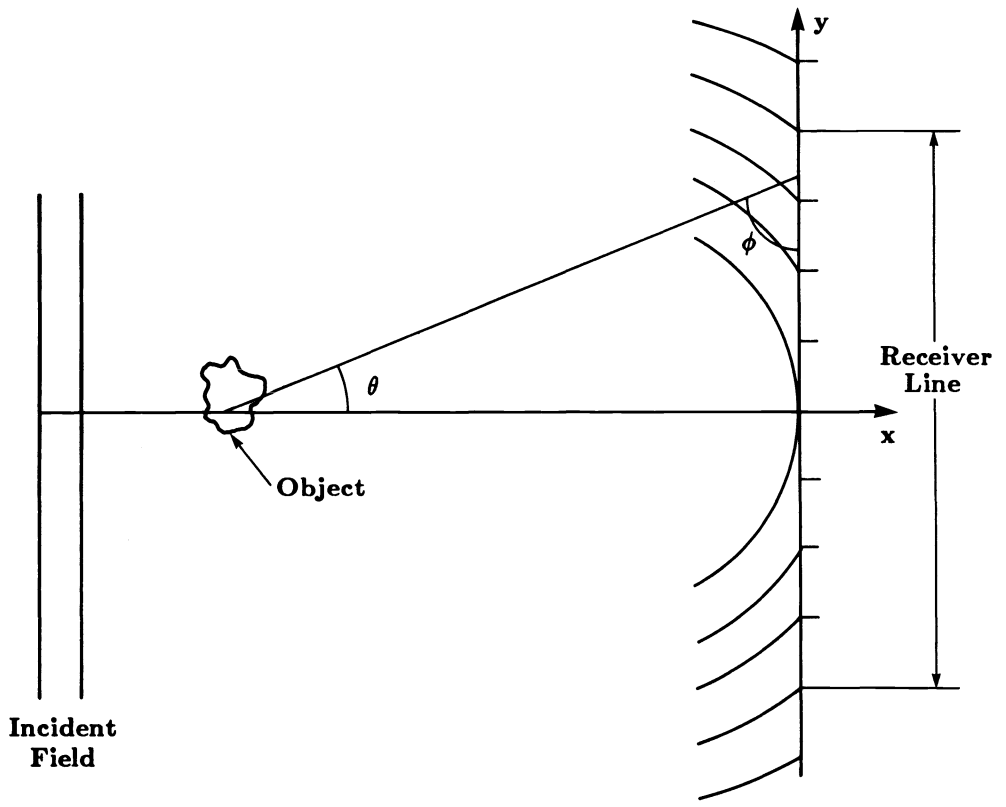

Figure 14. Schematic diagram of the receiver process for a single point scatterer.

[Gag78]. This results in

$$k_{recv}(x=l_0;y) = \frac{kl_0}{\sqrt{l_0^2+y^2}}. \tag{6.2}$$

Thus for a given receiver distance the maximum received frequency is a monotonically increasing function of length of the receiver line.

When sampling the diffracted projection with a constant number of points, N, there is a tradeoff between the sampling interval and the length of the receiver line. If, for example, the sampling interval is increased then more of the high frequency scattering information will be measured but the Nyquist rate will be lowered. By balancing the effect of sampling interval and receiver length it is possible to derive an estimate for the optimum sampling interval, T, as a function of the receiver's field of view, α, or

$$\alpha = \frac{x}{\lambda M} = \frac{2}{\tan\theta}. \tag{6.4}$$

Setting the Nyquist rate equal to equation (6.2) results in

$$\left[\frac{T}{\lambda}\right]^2 = \frac{\sqrt{64\alpha^2+1}+1}{8}. \tag{6.4}$$

Figure 15 shows the effect of varying the receiver sampling interval. The reconstructions shown are for a cylinder of radius 10λ and a refractive index of 1.01. The optimum sampling interval as predicted by equation (6.3) is 1.3λ.

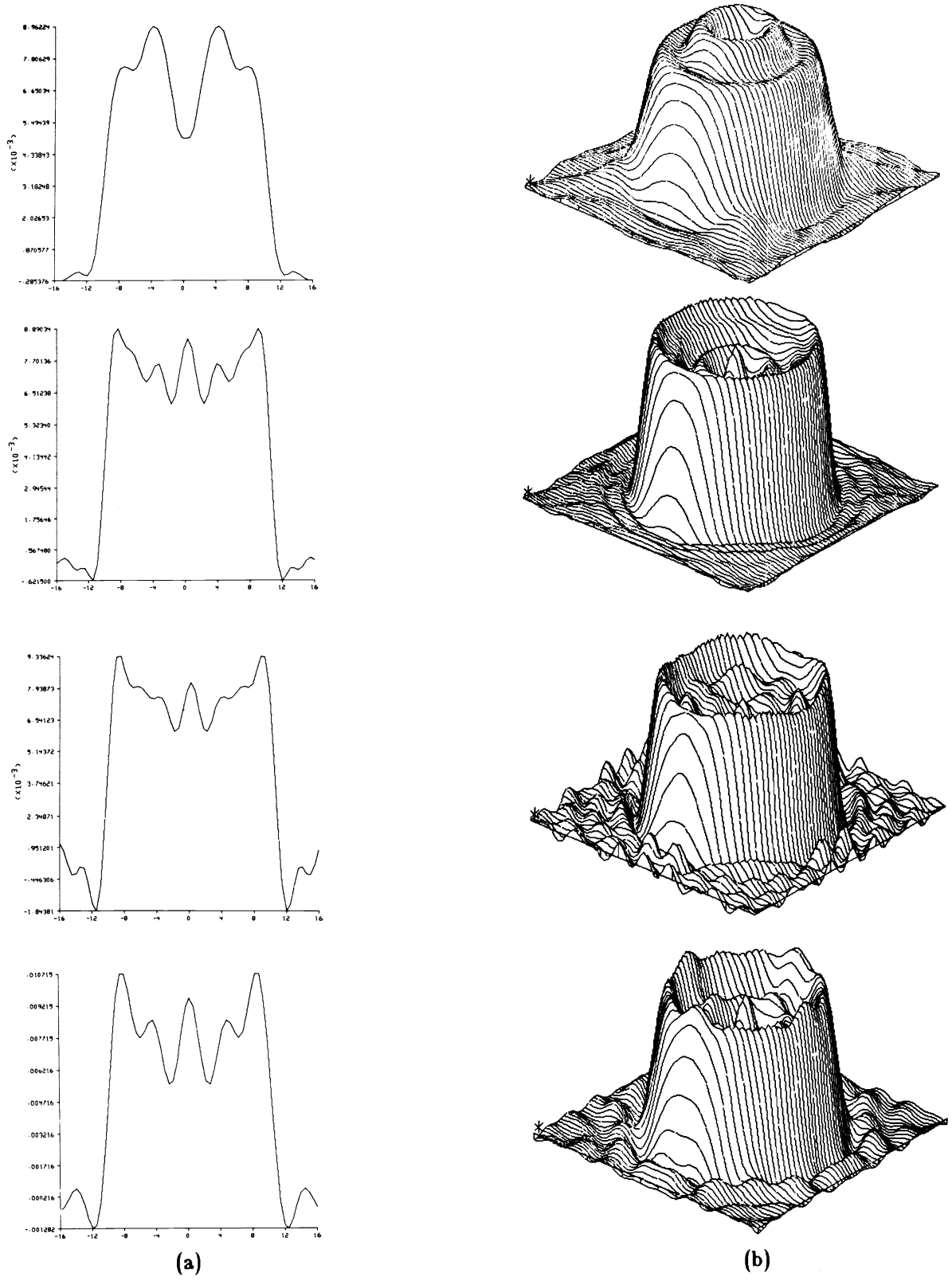

Figure 15. The effect of a finite receiver window. Optimum sampling interval is predicted by equation (6.4) as 1.3λ. The receiver line was 100λ from the object and was sampled at 64 positions. (a) Sampling interval is .5λ, (b) 1.0λ, (c) 1.5λ, (d) 2.0λ.

7. Conclusions

In this paper we have presented an overview of the state of diffraction tomography. The most severe limitation is due to the Born and Rytov approximations used to derive the forward scattering equations. In order to circumvent this limitation it will be necessary to derive better approximations to the field. One possibility is to use the higher order Born and Rytov approximations [Ish78].

We have also discussed two formulations of the diffraction tomography algorithm. These involve differences in the choice of incident fields and computations needed to perform the inversion.

We have also shown comparisons of reconstructions using interpolation and Devaney's backpropagation algorithm. The most significant difference was the large amount of time required to perform the reconstructions.

8. References

And82 A. H. Anders and A. C. Kak, "Digital Ray Tracing in Two-Dimensional Refractive Fields," *The Journal of the Acoustical Society of America,* Volume 72, Number 5, pp. 1593-1606, November 1982. *Optics Communications,* Volume 18, Number 4, pp 421-423, September 1976.

Che60 Lev A. Chernov "Wave Propogation in a Random Medium," McGraw-Hill Book Company, Inc, New York, 1960.

Cra82 Carl Crawford and A. C. Kak, "Multipath Artifacts in Ultrasonic Transmission Tomography," *Ultrasonic Imaging,* July 1982.

Dev82 A. J. Devaney, "A Filtered Backpropogation Algorithm for Diffraction Tomography," *Ultrasonic Imaging* 4, pp 336-350, 1982.

Gag78 R. Gagliardi, "Introduction to Communications Engineering," John Wiley and Sons, p. 28, 1978.

Goo68 J. W. Goodman, "Introduction to Fourier Optics," McGraw-Hill Book Company, San Francisco, 1968. *Acoustical Holography,* Volume II, 1981.

Ish78 Akira Ishimaru, "Wave Propogation and Scattering in Random Media," Academic Press, New York, NY, 1978.

Kak83 A. C. Kak, "Tomographic Imaging with Diffracting and Non-Diffracting Sources," in Array Processing Systems, edited by Simon Haykin, Prentice Hall, 1983 (in press).

Kel69 J. B. Keller, "Accuracy and Validity of the Born and Rytov Approximations," *Journal of the Optical Society of America,* Volume 59, pp. 1003-1004, 1969.

Mor53 Philip M. Morse and Herman Feshbach, "Methods of Theoretical Physics," Volume 1, McGraw-Hill Book Company, New York, NY, 1953.

Mor68 P. M. Morse and K. U. Ingard, "Theorectical Acoustics," McGraw-Hill Book Company, 1968.

Mue79 R. K. Mueller, Mostafa Kaveh and R. D. Iversen, "A New Approach to Acoustic Tomography Using Diffraction Techniques," Acoustical Imaging, Volume 8, Edited by A. Metherall, pp. 615-628.

Nah82 David Nahamoo and A. C. Kak, "Ultrasonic Diffraction Imaging," School of Electrical Engineering, Purdue University, TR-EE 82-20, 1982.

Pan83 S. X. Pan and A. C. Kak, "A Computational Study of Reconstruction Algorithms for Diffraction Tomography: Interpolation vs. Filtered-Backpropagation," To be Published in IEEE Transactions on Acoustics, Speech and Signal Processing.

Ros82 Azriel Rosenfield and Avinash C. Kak, "Digital Picture Processing," Academic Press, New York, Second Edition, 1982.

Sla82 Malcolm Slaney, "Limits in Diffraction Tomography," Purdue University, Internal Memo, 1982.

Wol69 E. Wolf, "Three-Dimensional Structure Determination of Semi-Transparent Objects from Holographic Data," *Optics Communications,* Volume 1, Number 4, pp. 153-156, 1969.